Impact of Virtual Synchronous Generators on Power System Frequency Dynamics

Aihui Fu, Aleksandra Lekić, Eleftherios O. Kontis, Kyriaki-Nefeli D. Malamaki, Georgios C. Kryonidis, Juan Manuel Mauricio, Charis S. Demoulias, Miloš Cvetković

***Abstract*—This paper deals with a systematic assessment of the power system frequency dynamics under high penetration of converter-interfaced renewable energy sources (CI-RESs). Specifically, the concept of the virtual synchronous generator (VSG) is implemented in the CI-RESs located at the transmission system (TS) side and/or the distribution network (DN) side. Dynamic RMS simulations are performed on a testbed consisting of the IEEE 9-bus TS grid and the CIGRE medium-voltage DN grid under different CI-RES penetration levels and VSG control parameters to assess the VSG impact on the power system frequency dynamics. It is shown that the decommissioning of conventional power plants coupled via synchronous generators can be safely performed in case the VSG concept is adopted correctly.**

***Index Terms*—Inertial response, primary frequency regulation, renewable energy resources, virtual synchronous generator.**

NOMENCLATURE

$CI-RESs$	Converter-interfaced renewable energy sources
DN	Distribution network
HV	High-voltage
IR	Inertial response
MV	Medium-voltage
PFR	Primary frequency response
SGs	Synchronous generators
TS	Transmission system
$VSGs$	Virtual synchronous generators

I. INTRODUCTION

A. Motivation and Background

FREQUENCY regulation has emerged as a significant challenge for transmission system operators (TSOs) in ensuring the security and stability of the grid [1]. To address this, TSOs traditionally relied on large conventional synchronous generators (SGs) to mitigate issues such as inertia shortage and primary frequency instability. However, with the increasing integration of converter-interfaced renewable energy sources (CI-RESs) directly connected to the transmission system (TS), grid codes now require these CI-RESs to participate in primary frequency regulation using power-frequency droop curves [2]. This transition has reduced system inertia and frequency reserves, primarily due to the displacement of SGs by CI-RESs lacking inherent inertia [3].

To address this challenge, the concept of virtual synchronous generators (VSGs) has emerged as a promising solution, enhancing the control of CI-RESs to provide inertial response (IR) and primary frequency response (PFR), thus emulating the behavior of traditional SGs [4].

Although several variants of the VSG model have been proposed in the literature [5]–[8], only a few studies evaluate their impact on the dynamic performance of power systems.

B. Relevant Literature

Specifically, in [9], a linearized model is introduced to analyze the oscillations of the grid. However, a simplified analysis is performed due to the small size of the examined network and the absence of SGs that could lead to possible interactions with CI-RESs. A small-scale grid is also assumed in [10] where simulations and hardware-in-the-loop experiments are conducted to evaluate the dynamic performance of the grid including both SGs and CI-RESs. In [11], a large TS is introduced to assess frequency dynamics under high CI-RES penetration.

Nevertheless, this analysis may lead to inaccurate results since the directly connected distribution networks (DNs) are modeled as passive loads neglecting their potential contribution to IR and PFR due to the increased penetration of CI-RESs equipped with VSG capabilities.

C. Contributions and Organization

This paper aims to fill this gap by including the CI-RESs' contribution at the DNs for assessing the power system frequency dynamics. To this end, dynamic RMS simulations are conducted on a testbed consisting of both TS and DN. Namely, the IEEE 9-bus TS and the CIGRE medium-voltage (MV) DN are used as examples. A parametric analysis is performed to evaluate the IR and PFR capabilities of CI-RESs under various penetration levels and different VSG control parameters.

The paper introduces the power system frequency dynamics assessment framework in Section II, and in Section III we conduct case studies to evaluate the ability of VSGs to provide an adaptable IR and PFR. The concluding remarks are presented in Section IV.

This research is funded by the European Union under the Horizon 2020 project EASY-RES (GA 764090).

A. Fu, A. Lekić, and M. Cvetković are with the Faculty of Electrical Engineering, Mathematics and Computer Science, Delft University of Technology, Delft, The Netherlands.

E. O. Kontis, K. N. Malamaki, G. C. Kryonidis, and C. S. Demoulias are with the Department of Electrical & Computer Engineering, Aristotle University of Thessaloniki, Thessaloniki, Greece.

J. M.Mauricio is with Department of Electrical Engineering, University of Seville, Spain.

Citation information, DOI: 10.1109/SEST57387.2023.10257357

II. Framework Build Up

A. Model Design in PowerFactory

To conduct the simulation and evaluation the PowerFactory is used. PowerFactory is a widely used commercial simulator that supports the simulation of transmission, distribution, generation, and distributed energy resources [12]. To get the influence of CI-RESs integration in the different voltage level networks, we connect TS and MV DN in the PowerFactory [12]. The simulated TS is depicted in Fig. 1, which is the IEEE 9 Bus Test System (WSCC Test Case) [13]. The simulated MV DN is presented in Fig. 2, the European benchmark CIGRE MV grid [14]. As shown in Figs. 1 and 2, CI-RESs are connected to both TS and DN, and The CIGRE MV DN is connected to bus 6 of the IEEE 9 Bus Test System. The network load parameters are shown in Table I.

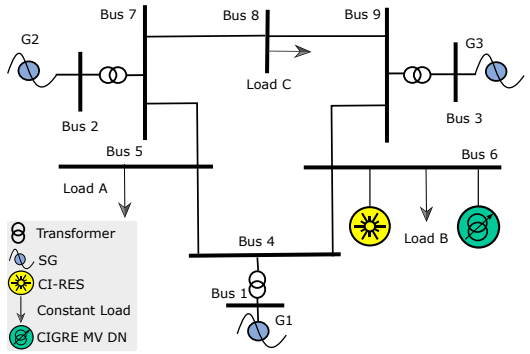

Fig. 1. IEEE 9-bus TS [15].

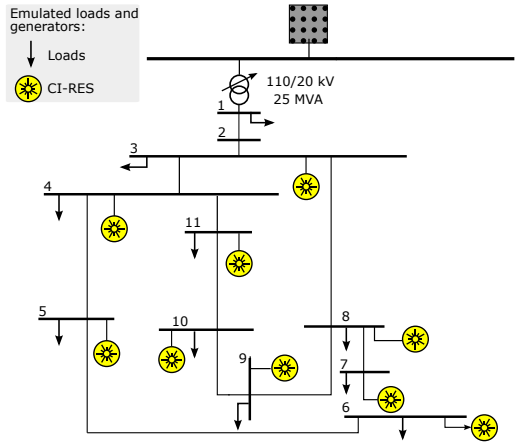

Fig. 2. CIGRE MV DN [14], [15].

This paper employs an enhanced version of the synchronous converter model VSGs to operate the CI-RESS. This control strategy was developed within the framework of the EU H2020 EASY-RES project and is detailed in [8], [16], where a proportional-integral controller is introduced to imitate the dynamic behavior of the conventional SGs. This controller is based on the principles of improved damping, decoupled power loops, and distinct handling of the IR and PFR. This approach allows for greater flexibility in the provision of both IR and PFR and ensures that the control of the CI-RESs is optimized for stable and reliable grid operation.

TABLE I
PARAMETERS IN THE BENCHMARK NETWORK

9-Bus HV network	
Node	Load apparent power[MVA]
Bus 5	175
Bus 8	135
Bus 6	22
CIGRE MV network	
Node	Load apparent power[MVA]
1	17.40
3	0,550
4	0,445
5	0,750
6	0,565
7	0,090
8	0,605
9	0,675
10	0,490
11	0,340

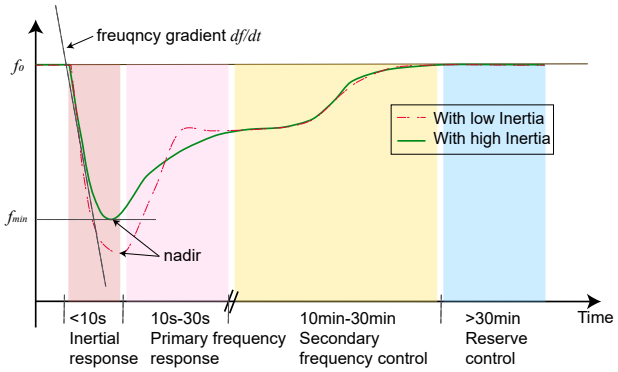

Fig. 3. Frequency response with under-frequency disturbance event.

B. Evaluation Items and Methods

To evaluate the IR and PFR, RMS is simulated in the PowerFactory. In the following simulations, the under-frequency and over-frequency disturbance events are modeled by increasing or decreasing the load. Fig. 3 illustrates the system frequency response to an under-frequency event. It is observed that the IR occurs within the first 10 seconds, while the PFR occurs between 10 and 30 seconds. A 1-millisecond integration step size is utilized in the simulation, with a total simulation time of 20 seconds and 60 seconds for the IR and PFR simulations, respectively.

The rate-of-change-of-frequency (ROCOF) is a critical parameter for evaluating IR. It is the derivative of the change in the grid frequency over time. It is an essential parameter in power systems as it indicates the system's stability. Low system inertia results in higher ROCOF values and lower frequency nadirs occurring in a shorter amount of time [17]. To assess power system stability with a high penetration of renewable energy, it is necessary to evaluate the ROCOF and

inertia constant by comparing the same contingencies. The ROCOF can be directly calculated using PowerFactory, and the equal inertia constant H_{eq} rated for all generators can be calculated based on Eq. (1).

$$H_{eq} = \frac{\sum_i^n H_i \cdot S_i}{\sum_i^n S_i}, \tag{1}$$

where H_{eq} is the equivalent inertia constant of all generators, H_i is the inertia constant of generator i, and S_i is the rated apparent power of generator i.

In terms of primary frequency control, the frequency droop control scheme is presented in Fig. 4. The parameters P_{max}, P_0, and DB in the Fig. 4 represent the available power, injected active power and the dead band of the primary frequency droop control, respectively. The primary frequency droop control's slope (S) is calculated using Eq. (2). It is active instantaneously when the frequency exceeds the dead band.

$$S(\%) = \frac{\Delta f}{f_n} \cdot \frac{Pmax}{\Delta P} \cdot 100 \tag{2}$$

Here, f_n is the base frequency 50Hz, Δf and ΔP are the deviation of frequency and active power.

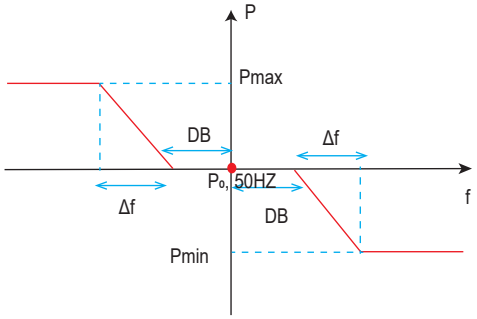

Fig. 4. The frequency droop control scheme.

III. Numerical Simulations

A. Case Study for Evaluating the IR

To evaluate whether the CI-RESs/VSGs can provide an adaptable IR, three simulation cases are presented and compared with each other:

- Case 1: The original network without any CI-RESs.
- Case 2: The original network with CI-RESs modeled as static generators, while one large generator is excluded.
- Case 3: Same configuration with Case 2, The IR is activated in the CI-RESs i.e., VSGs.

1) Parameters setting: Table II provides data on three SGs in the IEEE 9-Bus HV network for the three simulation cases. The installed capacity of the CI-RESs/VSGs in Case 2 and Case 3 in the CIGRE MV network is the same. The rated apparent power of CI-GRESs at Node 3, 4, 5, 6, 8, 9, 10, and 11 is 1 MVA, and CI-GRES at Bus 7 is 10 MVA. To determine if the developed VSGs can provide an adaptable IR when there is less IR from the SGs, generator G3 is disconnected in Case 2 and Case 3, and a single large CI-RESs generator (rated apparent power of 107 MVA) is added to Bus 6 of the IEEE 9-Bus HV network. In Case 3, the virtual inertia constant H for all VSGs is set to 5.

TABLE II
Parameters of SGs in the HV network

Parameters	G1	G2	G3
Rated Apparent power (MVA)	100	210	125
Inertia Constant H (s)	2,631	4,130	4,768

2) Evaluation results: In the simulation, the frequency change in the network is modeled by increasing Load A at Bus 5 of the HV TS by 60%. The network responses in the three examined cases are shown separately in Figs. 5, 6, and 7.

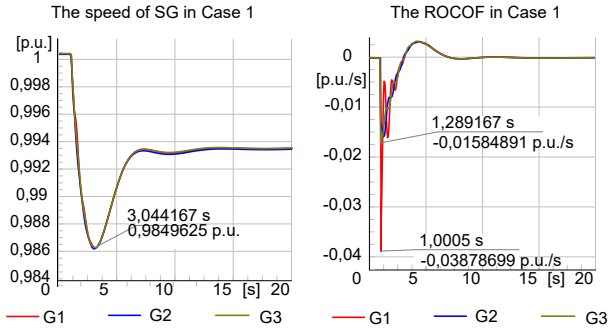

Fig. 5. IR in Case 1.

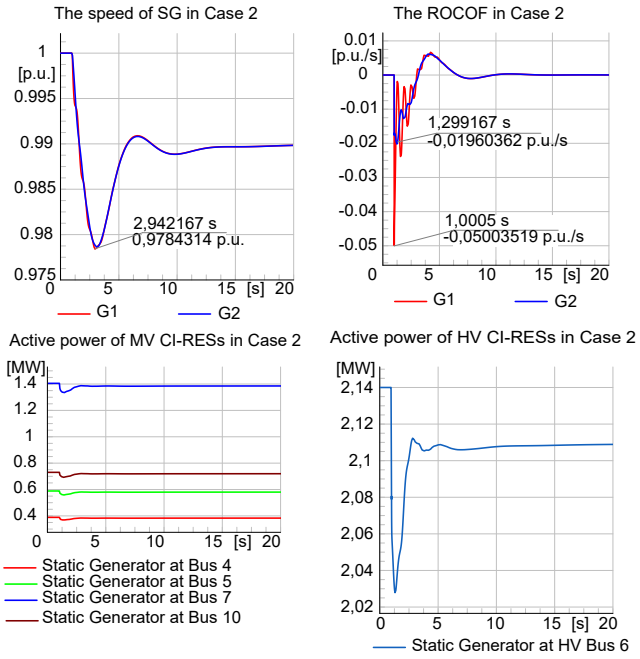

Fig. 6. IR in Case 2.

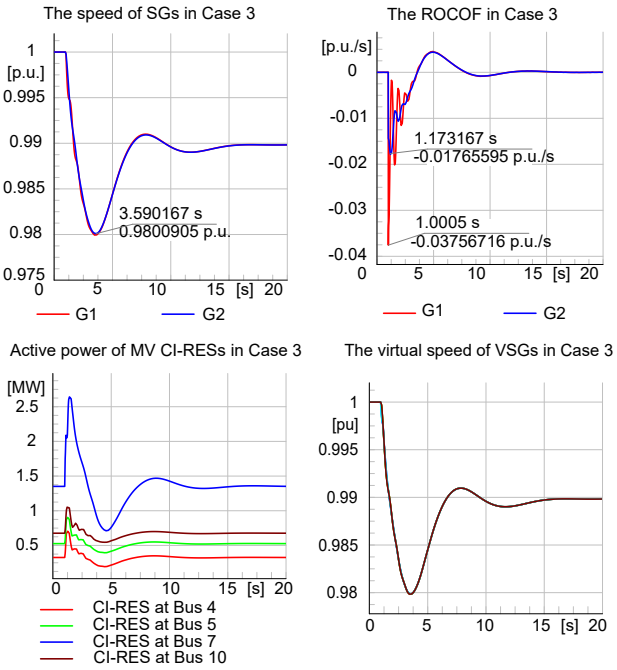

Fig. 7. IR in Case 3.

In this paper, we use changes in the speed of the generators to calculate ROCOF instead of changes in grid frequency because changes in the speed of the generators are more accurate and less susceptible to errors and noise than changes in grid frequency. As the simulation results show, the maximum absolute value of the derivative of the generator speed in Case 1 is 0.0388 p.u./s, in Case 2 is 0.05 p.u./s, while in Case 3 is 0.0376 p.u./s. This demonstrates that for the same contingency, the ROCOF increases by 28.9% (from 0.0388 p.u./s to 0.0500 p.u./s) with the increase in the penetration of static generators. On the other hand, if the CI-RESs are controlled with the VSG control, the ROCOF decreases by 3.09% (from 0.0388 p.u./s to 0.0376 p.u./s). The results demonstrate that the ROCOF decreases for the same contingency despite increased CI-RESs penetration. Based on the Eq. (1) and the parameters in Table II, H_{eq} of Case 1 is 3.969 seconds, Case 2 is 2.141 seconds, and Case 3 including the VSGs is 4.205 seconds. The inertia constant of Case 2 is smaller than that of Case 1 and Case 3, as the CI-RES do not have IR. Conversely, by introducing VSGs, the inertia constant of Case 3 is larger than that of the other cases. As a result, the frequency nadir in Case 2 (0.978 p.u.) is higher than in Case 3 (0.980 p.u.), indicating a greater deviation in the frequency response. Overall, these findings highlight the potential of VSGs to improve power system robustness and increase its resistance to abrupt frequency changes, even in high-penetration CI-RES scenarios. From the simulation results, we can get the following conclusion:

- VSGs can provide adaptable IR, which can be even larger than the conventional system.
- The ROCOF decreases for the same contingency with the increase in the VSGs penetration.
- By introducing virtual inertia in CI-RESs, the power system robustness can be increased towards abrupt frequency changes.

B. Case study for evaluating the PFR

In a power system with CI-RESs, ensuring stable PFR is essential to meet the technical requirements of system operators. Five cases are considered with both over-frequency and under-frequency events to evaluate the efficiency of the PFR.

TABLE III
DETAILED PARAMETERS OF EACH CASE

Case 0					
Parameters	G1	G2	G3	VSG	MVAL
$Pmax$[MW]	80	168	100	0	—
P_0[MW]	80	122.64	73	0	0
Q_0[MVar]	0	0	0	0	0
DB(Hz)	—	0	0	—	—
S(%)	—	3.7	3.7	—	—
Case 1-1					
Parameters	G1	G2	G3	VSG	MVAL
$Pmax$[MW]	80	168	0	68	32
P_0[MW]	80	122.64	0	48	25
Q_0[MVar]	0	0	0	0	0
DB(Hz)	—	0	—	0	0
S(%)	—	3.7	—	1.36	1.83
Case 1-2					
Parameters	G1	G2	G3	VSG	MVAL
$Pmax$[MW]	80	168	0	68	32
P_0[MW]	80	122.64	0	48	25
Q_0[MVar]	0	0	0	0	0
DB(Hz)	—	0	—	0	0,2
S(%)	—	3.7	—	1,36	1.83
Case 1-3					
Parameters	G1	G2	G3	VSG	MVAL
$Pmax$[MW]	80	168	0	68	32
P_0[MW]	80	122.64	0	48	25
Q_0[MVar]	0	0	0	0	0
DB(Hz)	—	0	—	0	0
S(%)	—	3.7	—	0,68	1.83
Case 2					
Parameters	G1	G2	G3	VSG	MVAL
$Pmax$[MW]	80	0	0	230	47
P_0[MW]	80	0	0	170	35
Q_0[MVar]	0	0	0	0	0
DB(Hz)	—	—	—	0	0
S(%)	—	—	—	2,3	2.35

1) Cases and parameter setting:

- Case 0: No CI-RESs are present; SGs G2 and G3 operate in Frequency Sensitive Mode (FSM) while G1 is fully loaded. The PFR is provided only from SGs.
- Case 1-1: One VSG is connected at HV network Bus 6, and four VSGs are connected at MV CIGRE network nodes 4, 5, 7 and 8 respectively. G1 is fully loaded, G2 operates in FSM mode, and G3 is disconnected. The frequency dead band of VSGs is set to 0, the droop slopes of the VSG connected at the HV network are set to 1.36% and the VSGs in the MV network are set to 1.83%.
- Case 1-2: This case is identical to Case 1-1. The only difference is in the dead band of VSGs which is set to 200 MHz.

- Case 1-3: This case is identical to Case 1-1. The only difference is the slope drop of the VSG in the HV network is set to 0.68%.
- Case 2: G1 is fully loaded, G2 and G3 are disconnected, and the installed capacity of VSGs is increased. The PFRs are all from VSGs. In contrast to all other cases, the limitation to the maximum primary frequency power of VSGs is set to ± 1 pu.

In all cases, the IR of VSGs is activated. The detailed parameters for each case are presented in Table III. MVAL denotes the generation of the CIGRE MV network and the VSG is used to provide the parameters of the VSG connected to the HV network, and P_{max}, P_0, Q_0 are the rated active power, the injected active power and the injected reactive power from the generators. For all cases, the active power for Load A, Load B, and Load C is set to 125 MW, 22 MW, and 100 MW, respectively, while their reactive powers are 50 Mvar, 0 Mvar, and 35 Mvar, respectively. The passive load of the CIGRE MV network is 25 MW for all cases. Case 0 represents the base case without CI-RESs. The SGs are partially replaced in Cases 1-1, 1-2, and 1-3. These cases evaluate the influence of the dead band and slope of droops of the PFR. In Case 2, the entire PFR is provided by VSGs. For all cases, the available power of the installed generators (SGs and/or VSGs) is 348 MW; The injected power, provided either by SGs or VSGs is for all cases 276 MW.

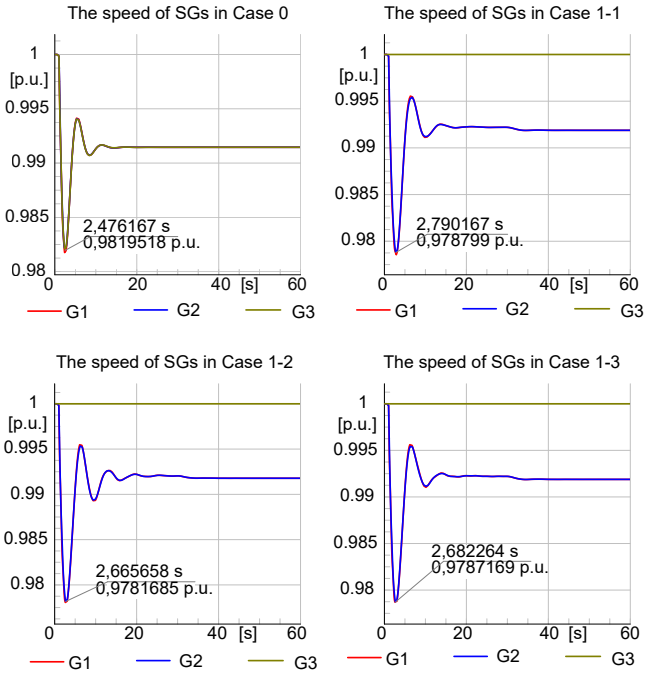

Fig. 8. Under-frequency simulation results in Case 0, Case 1-1, Case 1-2, and Case 1-3.

2) Evaluation results: An increase and decrease of 70 MW in Load C at bus 8 of the HV network are used to model under-frequency and over-frequency events, respectively. The results of the under-frequency response for the five cases are

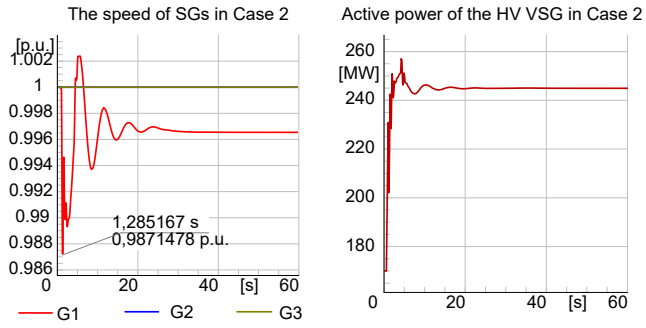

Fig. 9. Under-frequency simulation results in Case 2.

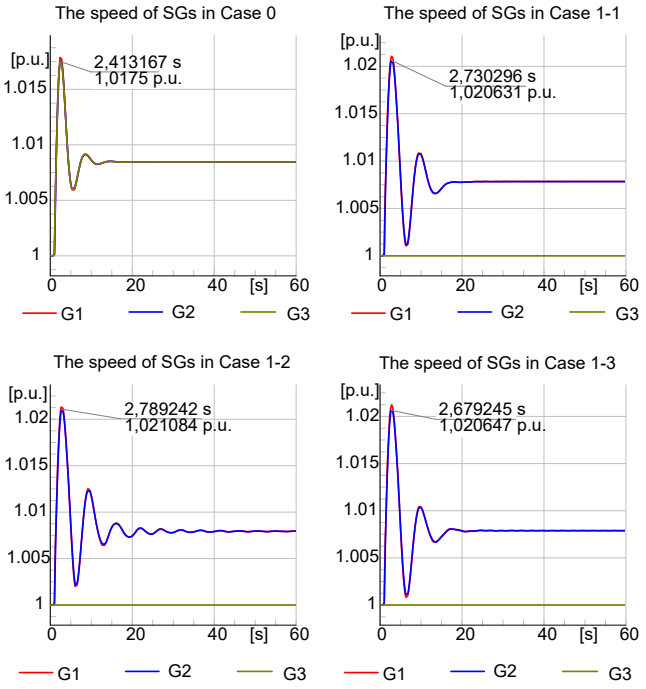

Fig. 10. Over-frequency simulation results in Case 0, Case 1-1, Case 1-2 and Case 1-3.

shown in Figs. 8 and 9. The simulation results show that the VSGs can increase their power output in response to the disturbance, stabilizing the frequency within approximately 30 seconds. A comparison of the frequency response between Case 1 and Case 0 reveals that G3 can be fully replaced by VSGs, resulting in almost the same frequency response. The impact of deadband and slope of the frequency control of VSGs on the frequency response is evaluated in Case 1-1, Case 1-2, and Case 1-3. A smaller droop control deadband allows the DRESs to respond more quickly to changes in frequency, leading to a faster adjustment in their power output. This helps in providing a more effective frequency regulation response. We can see that Case 1-2 uses more time than Case 1-1 to stabilize the frequency. Similarly, a higher slope of the droop control results in a more significant change in power output for a given change in frequency. This enables DRESs to contribute

more actively to frequency stability by quickly adjusting their power generation in response to frequency deviations. In Case 2, all SGs used for frequency regulation are replaced by VSGs, the only elements providing PFR. The nadir in Case 2 is 0.987 pu, demonstrating that VSGs have a better frequency response performance than Case 0 (0.982 p.u.).

The results of the over-frequency response in the five cases are presented in Figs. 10 and 11. The simulations of the over-frequency event yield the same conclusion as those of the under-frequency event. The VSGs, using improved VSG control, can effectively replace the reserves provided by SGs while achieving comparable or better PFR performance.

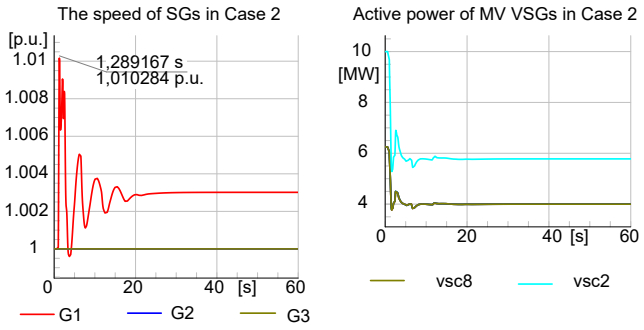

Fig. 11. Over-frequency simulation results in Case 2.

The simulation results have allowed us to verify the following three conclusions. Firstly, the VSGs exhibit an adaptable PFR that is either as good or superior to conventional SGs. Secondly, with adequate PFR, VSGs can fully replace conventional SGs. Lastly, to achieve optimal frequency response performance, the dead band and slope of the droop in VSGs frequency control must be appropriately set. In particular, the VSGs exhibit better frequency response performance with smaller dead bands and larger slopes of the droops.

IV. Conclusion

This paper provides a comprehensive analysis of the impact of VSGs on power system frequency dynamics in the presence of high levels of CI-RESs. The study employs dynamic RMS simulations on a testbed consisting of the IEEE 9-bus transmission system grid and the CIGRE medium-voltage distribution network grid, considering different levels of CI-RES penetration and VSG control parameters. A case study is presented to evaluate the IR of VSGs, which demonstrates that they can provide adaptable IR, which can be even greater than that of the conventional system. The study also shows that the rate of change of frequency ROCOF decreases with the increase in VSGs penetration, indicating that introducing virtual inertia in CI-RESs can increase the power system's robustness against abrupt frequency changes.

Additionally, the paper presents a case study to evaluate the PFR of VSGs, which reveals that they exhibit controllable PFR that it can be considered superior to conventional SGs. It is essential to set the dead band and slope of the droop in VSGs frequency control appropriately to achieve optimal frequency response performance.

The findings of this study can guide the development and implementation of effective control strategies for high penetration of CI-RESs in power systems, which can enhance their stability and reliability.

References

[1] E. O. Kontis, A. R. d. Nozal, J. M. Mauricio, and C. S. Demoulias, "Provision of primary frequency response as ancillary service from active distribution networks to the transmission system," *IEEE Trans. Smart Grid*, vol. 12, no. 6, pp. 4971–4982, 2021.

[2] "Ieee standard for interconnection and interoperability of distributed energy resources with associated electric power systems interfaces," *IEEE Std 1547-2018 (Revision of IEEE Std 1547-2003)*, pp. 1–138, 2018.

[3] F. Arredondo, P. Ledesma, E. D. Castronuovo, and M. Aghahassani, "Stability improvement of a transmission grid with high share of renewable energy using TSCOPF and inertia emulation," *IEEE Trans. Power Syst.*, vol. 37, no. 4, pp. 3230–3237, 2022.

[4] B. Long, S. Zhu, J. Rodriguez, J. M. Guerrero, and K. t. Chong, "Enhancement of power decoupling for virtual synchronous generator: A virtual inductor and virtual capacitor approach," *IEEE Trans. Ind. Electron.*, pp. 1–13, article in press.

[5] M. Chen, D. Zhou, and F. Blaabjerg, "Modelling, implementation, and assessment of virtual synchronous generator in power systems," *J. Modern Power Syst. Clean Energy*, vol. 8, no. 3, pp. 399–411, 2020.

[6] L. Tao, X. Zha, Z. Tian, and J. Sun, "Optimal virtual inertia design for vsg-based motor starting systems to improve motor loading capacity," *IEEE Transactions on Energy Conversion*, vol. 37, no. 3, pp. 1726–1738, 2022.

[7] H. Liu, D. Sun, P. Song, X. Cheng, F. Zhao, and Y. Tian, "Influence of virtual synchronous generators on low frequency oscillations," *CSEE Journal of Power and Energy Systems*, vol. 8, no. 4, pp. 1029–1038, 2020.

[8] S. Bu, "Investigation on impact of virtual synchronous generator and its auxiliary controller on power system frequency and oscillation stability," 2019.

[9] P. Sun, J. Yao, Y. Zhao, X. Fang, and J. Cao, "Stability assessment and damping optimization control of multiple grid-connected virtual synchronous generators," *IEEE Trans. Energy Conv.*, vol. 36, no. 4, pp. 3555–3567, 2021.

[10] B. Long, Y. Liao, K. T. Chong, J. Rodríguez, and J. M. Guerrero, "MPC-controlled virtual synchronous generator to enhance frequency and voltage dynamic performance in islanded microgrids," *IEEE Trans. Smart Grid*, vol. 12, no. 2, pp. 953–964, 2021.

[11] M. Zhao, H. Yin, Y. Xue, X.-P. Zhang, and Y. Lan, "Coordinated damping control design for power system with multiple virtual synchronous generators based on prony method," *IEEE Open Access J. Power Energy*, vol. 8, pp. 316–328, 2021.

[12] D. PowerFactory, "Digsilent powerfactory 2021 user manual," *DIgSILENT GmbH 2021*, 2021.

[13] A. R. Al-Roomi, "Power Flow Test Systems Repository," Halifax, Nova Scotia, Canada, 2015. [Online]. Available: https://al-roomi.org/power-flow

[14] CIGRE, "Benchmark systems for network integration of renewable and distributed energy resources," *CIGRE Task Force C6.04.02*, 2014.

[15] K.-N. D. Malamaki, S. Giazitzis, S. Gkavanoudis, A. Fu, a. J. M. M. Aleksandra Lekić, E. Kontis, C. Demoulias, and M. Cvetković, "D6.5 report on the evaluation of project KPIs," *H2020 EASY-RES Project Deliverable*, Dec. 2021.

[16] G. C. Kryonidis, K-N. D. Malamaki, J. M. Mauricio, and C. S. Demoulias, "A new perspective on the synchronverter model," *Int. J. Electr. Power Energy Syst.*, vol. 140, 2022.

[17] P. Tielens and D. Van Hertem, "The relevance of inertia in power systems," *Renewable and Sustainable Energy Reviews*, vol. 55, pp. 999–1009, 2016.